Atmos. Chem. Phys. Discuss., 6, 10773–10809, 2006
www.atmos-chem-phys-discuss.net/6/10773/2006/

Atmospheric Chemistry and Physics Discussions

The role of the retention coefficient for the scavenging and redistribution of highly soluble trace gases by deep convective cloud systems: model sensitivity studies

M. Salzmann[1], M. G. Lawrence[1], V. T. J. Phillips[2], and L. J. Donner[2]

[1]Max-Planck-Institute for Chemistry, Department of Atmospheric Chemistry, PO Box 3060, 55020 Mainz, Germany
[2]Geophysical Fluid Dynamics Laboratory, NOAA, Princeton University, PO Box 308, Princeton, NJ 08542, USA

Received: 19 September 2006 – Accepted: 20 October 2006 – Published: 24 October 2006

Correspondence to: M. Salzmann (salzmann@mpch-mainz.mpg.de)

Abstract

The role of the retention coefficient (i.e. the fraction of a dissolved trace gas which is retained in hydrometeors during freezing) for the scavenging and redistribution of highly soluble trace gases by deep convective cloud systems is investigated using a modified version of the Weather Research and Forecasting (WRF) model. Results from cloud system resolving model runs (in which deep convection is initiated by small random perturbations in association with so-called "large scale forcings (LSF)") for a tropical oceanic (TOGA COARE) and a mid-latitude continental case (ARM) are compared to two runs in which bubbles are used to initiate deep convection (STERAO, ARM). In the LSF runs scavenging is found to almost entirely prevent a highly soluble tracer initially located in the lowest 1.5 km of the troposphere from reaching the upper troposphere, independent of the retention coefficient. The release of gases from freezing hydrometeors leads to mixing ratio increases in the upper troposphere comparable to those calculated for insoluble trace gases only in runs in which bubbles are used to initiate deep convection. This result indicates that previous cloud resolving model studies using bubbles to initiate deep convection may possibly have over-estimated the influence of the retention coefficient on the vertical transport of highly soluble tracers. The retention coefficient is, however, found to play an important role for the scavenging and redistribution of highly soluble trace gases with a (chemical) source in the free troposphere and also for trace gases for which even relatively inefficient transport may be important.

1 Introduction

Deep convective clouds can rapidly transport trace gases from the lower to the upper troposphere (e.g. Isaac and Joe, 1983; Chatfield and Crutzen, 1984; Dickerson et al., 1987) where in many cases their chemical lifetimes are longer, and, especially at mid-latitudes, horizontal winds are generally stronger. Highly soluble trace gases, on the

ACPD

6, 10773–10809, 2006

other hand, are efficiently scavenged due to uptake in liquid hydrometeors and subsequent removal by precipitation (e.g. Hales and Dana, 1979; Wang and Crutzen, 1995; Crutzen and Lawrence, 2000). A few recent model studies (Crutzen and Lawrence, 2000; Mari et al., 2000; Barth et al., 2001; Yin et al., 2002) have, however, suggested that even highly soluble trace gases can reach the upper troposphere if they are released from freezing hydrometeors at high altitudes. In a cloud resolving model study of a mid-latitude storm, Barth et al. (2001) found that when soluble trace gases were assumed to be released from hydrometeors upon freezing, both low and high solubility tracers were transported to the upper troposphere. When the tracers were assumed to be retained in ice hydrometeors, the highly soluble tracers were not ultimately transported to the upper troposphere, but precipitated out instead. Using an axis-symmetric cloud model with a size-bin-resolving microphysics scheme, Yin et al. (2002) also found the deep convective transport of highly soluble trace gases to depend on the retention coefficient, especially under maritime conditions. Based on results from a one-dimensional entraining/detraining plume model, Mari et al. (2000) suggested that inefficient scavenging of hydrogen peroxide (H_2O_2) in glaciated clouds may explain the observations of enhanced H_2O_2 in outflow from deep convection. Whether H_2O_2 is completely scavenged in deep convection because of its high solubility or whether some H_2O_2 is injected into the upper troposphere during hydrometeor freezing could potentially play an important role for the HO_x(=HO_2 + OH) budget of the upper troposphere (Chatfield and Crutzen, 1984; Prather and Jacob, 1997; Jaeglé et al., 1997). In the present study, the influence of the retention coefficient on the transport and scavenging of idealized, highly soluble tracers with various initial profiles is investigated. Direct uptake on ice from the gas phase is not considered. The following two sections provide a description of the model and an overview of the meteorological aspects of the simulations. Results for the transport and scavenging of highly soluble tracers with two different initial profiles are presented in Sect. 4. The influences of the simulated cloud dynamics and microphysics on the transport are investigated in Sect. 5. In Sect. 6, the results are discussed in light of observed increases of upper tropospheric H_2O_2 mixing

ratios in deep convective outflow. In order to reconcile our results with the observations, results from additional sensitivity runs are presented.

2 Model description

A modified height coordinate prototype version of the non-hydrostatic, compressible Weather and Research and Forecast Model (WRF) is used in this study. The WRF model is a community model which is being developed in a collaborative effort by the National Center for Atmospheric Research (NCAR), the National Centers for Environmental Prediction (NCEP), the Air Force Weather Agency, Oklahoma University, and other partners. It was designed as a regional model which is capable of operating at high resolutions. The source code as well as additional information can be obtained from the WRF model web site at http://wrf-model.org. The basic equations can be found in Skamaraock et al. (2001) and the numerics are described in Wicker and Skamarock (2002). In the present study, microphysical processes are parameterized using a single-moment scheme based on Lin et al. (1983) which is not part of the WRF model distribution. The scheme is described by Krueger et al. (1995) and is based on a study by Lord et al. (1984). The mass mixing ratios of water vapor, cloud water, rain, cloud ice, graupel, snow, and tracers are transported using the Walcek (2000) monotonic advection scheme instead of the third order Runge-Kutta scheme which was originally implemented in the WRF model prototype. The densities for cloud ice, snow, and graupel are set to ρ_i=917 kg m^{-3}, ρ_s=100 kg m^{-3}, and ρ_g=400 kg m^{-3}, respectively. The intercept parameters of the Marshall–Palmer size distributions for rain, snow, and graupel are $n_{0r}=8\times10^6$ m^{-4}, $n_{0s}=3\times10^6$ m^{-4}, $n_{0g}=4\times10^6$ m^{-4}; and the radius of the model cloud ice particles is r_i=50 μm. The third order Runge-Kutta scheme is used to solve the momentum equations and the theta equation using fifth/third order spatial discretizations for horizontal/vertical advection terms. Shortwave radiation is parameterized using the Goddard shortwave scheme (Chou et al., 1998) and the RRTM scheme (Mlawer et al., 1997) is used for parameterizing longwave radiation

in the simulations. Subgrid scale turbulence is parameterized applying Smagorinsky's closure scheme (e.g. Takemi and Rotunno, 2003) except in the STERAO run, where K-theory with constant horizontal (K_h=100 m^2 s^{-1}) and vertical (K_v=1 m^2 s^{-1}) coefficients is used (see discussion in Sect. 3.3).

For soluble trace gases the uptake by, release from, sedimentation together with, and mass transfer between different model categories of hydrometeors in the liquid or ice phase are calculated. Neither gas nor aqueous phase reactions are considered. Concentrations of dissolved trace gases and gases taken up by the ice phase are treated as prognostic variables (i.e. they undergo transport and parameterized turbulence). The rate of change of the gas phase concentration C_g due to uptake/release of a tracer by/from hydrometeors is

$$\partial_t C_g|_{hy} = -\sum_{j=1}^{5} \left(\partial_t C_j|_{mt} - \partial_t C_j|_{ev,su}\right), \quad (1)$$

where $\partial_t C_j|_{mt}$ is the rate for the mass transfer between hydrometeors of category j and the gas phase (for release $\partial_t C_j|_{mt}$<0), and $\partial_t C_j|_{ev,su}$ is the source rate due to the evaporation or sublimation of hydrometeors of model category j. $\partial_t C_j|_{ev,su}$ is zero unless hydrometeors of a certain category entirely evaporate or sublimate during an integration timestep. In this case, the tracer is assumed to be completely released to the gas phase (aerosol effects, in particular sticking to the condensation nucleus are not considered). The rate of change (in addition to advection and turbulence) of the concentration C_j (defined per grid box volume) of a tracer taken up by hydrometeors of model category j is

$$\partial_t C_j|_{hy} = \partial_t C_j|_{mt} + \partial_t C_j|_{\text{sed}} + \partial_t C_j|_{mp} - \partial_t C_j|_{ev,su}, \quad (2)$$

where $\partial_t C_j|_{\text{sed}}$ is the rate due to transport together with sedimenting hydrometeors, and $\partial_t C_j|_{mp}$ is the rate due to mass transfer between different hydrometeor categories.

The uptake and release of trace gases is assumed to be limited by the mass transfer across the interface of the hydrometeors and by the diffusion of the trace gas in

the air surrounding the meteors and is parameterized using first-order rate coefficients (Schwartz, 1986). The rate of change of the aqueous phase concentration for hydrometeor category j is

$$\partial_t C_j|_{mt} = f_j k_j L_j C_g - \frac{f_j k_j}{K_H RT} C_j, \tag{3}$$

where f_j is the ventilation coefficient, L_j is the liquid water volume fraction of hydrometeors of category j, K_H is the (usually temperature dependent) Henry's Law coefficient, T is the temperature, and R the universal gas constant. Subsequently the indices i and j will be dropped. The first order rate constant k is calculated from:

$$k = \left(\tau_{Dg} + \tau_{\text{int}}\right)^{-1}, \tag{4}$$

where τ_{Dg} is a characteristic timescale for gas diffusion and τ_{int} is a characteristic timescale for the mass transfer across the interface of a hydrometeor:

$$\tau_{Dg} = \frac{\overline{a}^2}{3D_g}, \quad \tau_{\text{int}} = \frac{4\overline{a}}{3\nu\alpha_{\text{acc}}}, \tag{5}$$

where $\overline{a}$ is the mass mean radius of the hydrometeors, D_g is the gas phase diffusivity of the trace gas, α_{acc} is the gas-dependent mass accommodation coefficient (the fraction of collisions resulting in uptake) and $\nu = \sqrt{8RT/\pi M}$ is the mean molecular velocity, where M is the molar mass of the trace gas. For the mass transfer calculations $\overline{a}$=10 μm for cloud droplets, and $\overline{a}=2/\lambda$ for rain drops, where λ is the slope of the raindrop size distribution calculated in the microphysics scheme. The gas phase diffusivity is calculated from (Massman, 1998):

$$D_g(T,\rho) = D^0_{H_2O} \sqrt{\frac{M_{H_2O}}{M}} \left(\frac{\rho_0}{\rho}\right) \left(\frac{T}{T_0}\right)^{1.81}, \tag{6}$$

where the index 0 indicates values at T_0=273.15 K and p_0=1013 hPa. Typical gas phase diffusivities are of the order of 0.1 $cm^2\,s^{-1}$.

In deriving Eq. (6) the assumption was used that the diffusivity of a particular gas with molar mass M_u can be inferred by scaling a measured diffusivity of a gas with molar mass M_k by $\sqrt{M_k/M_u}$. This assumption can lead to errors up to 23% (Massman, 1998). The ventilation coefficient is calculated from the empirical expression (Pruppacher and Klett, 1997):

$$f = 0.78 + 0.308\, N_{Sc,v}^{1/3} N_{Re}^{1/2}, \tag{7}$$

where N_{Sc}=ν_a/D_g is the Schmidt number and N_{Re}≈$2\overline{u}_\infty \overline{a}/\nu_a$ is the Reynolds number, with ν_a being the kinematic viscosity of air and u_∞ the terminal velocity of the hydrometeors.

Following Barth et al. (2001), the sedimentation rate is calculated using the mass weighted mean terminal velocity $\overline{u}_{\infty j}$ (positive downwards, where the index j is included again to emphasize the dependence on hydrometeor category) of the falling hydrometeors (all except cloud droplets, where sedimentation is neglected):

$$\partial_t C_j|_{\text{sed}} = \partial_z \left(\overline{u}_{\infty j} C_j\right). \tag{8}$$

The mass transfer between different hydrometeor categories is assumed to be proportional to the mass transfer of liquid or frozen water between the different categories as calculated by the microphysics parameterization:

$$\partial_t C_j|_{mp} = k_{\text{ret}_i} \sum_{k=1}^{5} \left(R_{k,j} \frac{C_k}{q_k} - R_{j,k} \frac{C_j}{q_j} \right), \tag{9}$$

where $R_{k,j}$=$\partial_t q_j|_{k\to j}$ is the rate of liquid or frozen water transfer from meteors of category k to meteors of category j due to a microphysical process; k_{ret} is a dimensionless retention fraction and is one for all processes except freezing and riming. The retention

coefficient is assumed to be independent of whether wet or dry growth riming or homogeneous freezing occur. Effects of the so-called quasi-liquid layer (e.g. Diehl et al., 1995) (of which the structure is still largely unknown) are not considered.

3 Model setup and meteorological overview

In multi-day cloud system resolving studies, so-called "large scale forcings" based on Soong and Ogura (1980) are added to the thermodynamic equation and to the equation for water vapor in order to represent the influences of larger scale dynamics which are not resolved by typical limited area cloud resolving models:

$$\left(\frac{\partial\overline{\theta}}{\partial t}\right)_{LS} = -\overline{\boldsymbol{v}}\cdot\nabla\overline{\theta} - \overline{w}\frac{\partial\overline{\theta}}{\partial z} \tag{10}$$

$$\left(\frac{\partial\overline{q}}{\partial t}\right)_{LS} = -\overline{\boldsymbol{v}}\cdot\nabla\overline{q} - \overline{w}\frac{\partial\overline{q}}{\partial z}, \tag{11}$$

where $\boldsymbol{v}=(u,v)$ is the horizontal wind vector, q is the water vapor mixing ratio, θ is the potential temperature, and overbars denote horizontal domain averages. The large scale forcings for q and θ in Eqs. (10) and (11) are derived from comprehensive observation campaigns. The gradients of $\overline{q}$, $\overline{\theta}$, and $\overline{w}$ depend to some extent on the deep convection taking place inside the domain, which is important to note when using the traditional term "large scale forcings". In the multi-day cloud system resolving model runs, the average horizontal wind is nudged towards observed values:

$$\left(\frac{\partial\overline{\boldsymbol{v}}}{\partial t}\right)_{LS} = -\frac{\overline{\boldsymbol{v}}-\overline{\boldsymbol{v}}_{\mathrm{obs}}}{\tau_{\mathrm{adj}}} \tag{12}$$

as in e.g. Xu and Randall (1996) with an adjustment time $\tau_{\mathrm{adj}}=1$ h.

In the following, results from 3-D runs with periodic lateral boundary conditions are presented. For TOGA COARE (19–26 December 1992) and ARM A (26–30 June 1997)

results from cloud system resolving multi-day runs with prescribed "large scale forcings" for q and θ and surface skin temperatures are presented. In these runs very small (maximum 0.1 g kg^{-1}) water vapor perturbations are applied during the first 2.5 h of the simulations (prior to the onset of deep convection). The STERAO run is initialized with three positively buoyant thermals ("bubbles") as in Barth et al. (2001) and the model was run for 2.5 h. Furthermore, a short term (2.5 h) run was initialized on 29 June 1997, 23:30 GMT with meteorological profiles from ARM A in which a positively buoyant ($\Delta\theta_{max}$=5 K) thermal with radius r=20 km and height z_o=1800 m was used to initiate deep convection. The horizontal domain size used in all runs is 278×278 km^2 and the horizontal resolution is 2 km. The vertical resolution is 350 m in the TOGA COARE runs and variable grid spacings with increasing resolution towards the Earth's surface are used in the ARM and the STERAO runs. The timestep is 5 s in all runs. In the multi-day runs, the tracer fields are reset to their (horizontally homogeneous) initial values every 24 h after an initial offset of 12 h, and the lateral boundary conditions for the tracers are periodic. A vertical large scale advection tendency for tracers (VLSAT, Salzmann et al., 2004) was not applied. The Henry's law coefficients of the soluble tracers are set to $H_L = 1 \times 10^6$ mol l^{-1} atm^{-1} independent of temperature (i.e. the tracers are highly soluble and increases of H_L with height due to decreasing temperatures are not taken into account). The accommodation coefficient is set to α_{acc}=0.2 and the molar mass of the idealized tracers is set equal to the molar mass of HNO_3 in all sensitivity runs. In addition to the 3-D runs, 2-D sensitivity runs have been conducted, which will be described in Sect. 6.

3.1 The TOGA COARE case

A seven day episode from 19–26 December 1992 at the site of the Tropical Ocean Global Atmospheres/Coupled Ocean Atmosphere Response Experiment (TOGA COARE, Webster and Lukas, 1992) Intensive Flux Array (IFA, centered at 2° S, 156° E in the tropical West Pacific) is modeled, which has been extensively studied using cloud system resolving models (e.g. Johnson et al., 2002; Gregory and Guichard, 2002). This

episode was also studied by Salzmann et al. (2004) using the same model setup with a smaller 3-D domain and specified lateral boundary conditions for water vapor. On the whole the meteorological results from the TOGA COARE run in the present study are similar to the results presented by Salzmann et al. (2004), and the reader is referred to Salzmann et al. (2004) for a description of the meteorological conditions.

3.2 The ARM runs

The Atmospheric Radiation Measurement Program (ARM) case (ARM A, 26–30 June 1997, Southern Great Plains) is also well documented and has been studied e.g. in an intercomparison of various cloud system resolving models (Xu et al., 2002). The data used for specifying the "large scale forcing" terms in the present study as well as data from observations were obtained from http://kiwi.atmos.colostate.edu/scm/arm-data/jul97.html (Version 2 datasets, Zhang et al., 2001).

Figure 1 shows good agreement for simulated and observed 6 h average surface precipitation rates for the ARM A period. The accumulated rainfall for the entire episode is 31.5 mm in the simulations and 32.9 mm in the observations. Figure 2c shows that the maximum rain rates coincide with the development of longer lived mesoscale systems. The domain average simulated cloud liquid water path (excluding the first day) is 37.9 g m^{-2} and the average cloud ice water path (excluding the first day) is 13.7 g m^{-2}. Both values are at the lower end, but still inside the wide range reported by Xu et al. (2002) for various other cloud system resolving models. The differences between time and horizontally domain averaged modeled and observed temperatures and water vapor mixing ratios are shown in Fig. 3. Height dependent biases of similar magnitude have also been found in other cloud system resolving studies and are not only model, but too a large extent also case dependent. The ARM run was performed with increasing vertical grid resolution towards the Earth's surface. Increasing the resolution in the lower model layers was found to result in an earlier onset of deep convection in better agreement with the observations. Increasing the resolution in a TOGA COARE sensitivity run, on the other hand, resulted in very small changes of the modeled trace gas

transport (not shown), and therefore the TOGA COARE run was performed with constant vertical resolution. The relatively warm bubble in the ARM A bubble ("ARM BUB") run resulted in a relatively short lived single cell storm (Fig. 2b) with a top below 12 km above ground level (AGL), while the cloud tops in the run with large scale forcings were higher (see Sect. 5). This reflects the importance of the large scale forcings in the ARM case.

3.3 The STERAO case

The 10 July 1996, Stratospheric-Tropospheric Experiment: Radiation, Aerosols, and Ozone (STERAO) case has previously been studied using a cloud resolving model by Skamarock et al. (2000) and Barth et al. (2001). Figure 2a gives an impression of the evolution of the simulated storm. Some details are discussed in Sect. 5. For numerical stability reasons, the STERAO case was run with constant eddy diffusion coefficients. In order to asses how this choice affects the results of the present study, a sensitivity run with the same eddy diffusion coefficients was performed for ARM. Using constant eddy diffusion coefficients for the ARM case did not change the results from this study significantly (not shown).

4 Transport of highly soluble tracers

Figure 4a shows horizontally averaged mixing ratio profiles calculated for two different initial profiles (T1 and T2) for the TOGA COARE case. The tracers with initial profiles T1 are initially located in the lower troposphere, while the initial profile of T2 is a CO profile which has been used by Barth et al. (2001) in their pioneering cloud resolving model study of soluble tracer transport during STERAO. The tracers have been assumed to be either insoluble, highly soluble and completely retained during hydrometeor freezing, or highly soluble and completely released during hydrometeor freezing. While the insoluble tracers are efficiently transported to the upper troposphere, scav-

ACPD
6, 10773–10809, 2006

EGU

enging prevents efficient transport for the soluble tracers independent of the retention coefficient. This is also the case for the ARM A LSF run (Figs. 4b and 5). In Sect. 5 it will be shown that in these runs, highly soluble tracers with initial profile T1 are efficiently scavenged already below the 0°C level. The strong sensitivity of tracers with initial profle T2 to the retention cofficient suggests that the retention coefficient plays a large role for the scavenging of highly soluble trace gases with a (chemical) source in the upper troposphere. In the lower troposphere, slightly higher mixing ratios of "T2 retained" compared to "T2 released" are due to more dissolved tracer being released from evaporating hydrometeors.

Based on the ratios $\alpha = \overline{\mu}_s / \overline{\mu}_i$ of soluble to insoluble tracer average mixing ratios in the upper troposphere after modelled deep convection, Barth et al. (2001) have suggested that global models such as the one used by Crutzen and Lawrence (2000) may underestimate the transport of highly soluble tracers to the upper troposphere. Crutzen and Lawrence (2000), however, investigated the transport of soluble tracers with a surface source (similar to T1), while the initial profile specified by Barth et al. (2001) is identical to T2. Based on Fig. 4, and on Table 1, one can attribute the difference noted by Barth et al. (2001) to the use of different initial/boundary conditions in the two studies.

Table 1 shows ratios α for the TOGA COARE and ARM multiday runs based on averages over the output times 2.5 h after the onset of deep convection (defined as the first output time when the maximum total hydrometeor mixing ratio at a single grid point above 7 km exceeds 1 g kg^{-1}), and 12 h, and 24 h after each re-initialization. The upper troposphere is defined as the region 7–16 km altitude for TOGA COARE, and 7–14 km for the mid-latitude cases. Furthermore, the table shows the ratios at the end of the simulation (after 2.5 h) for the STERAO and the ARM BUB case which were initialized with positively bouyant thermals as described in the previous section. Note that especially for T2 the ratios generally depend on domain size, since they depend on the ratio of cloudy area to cloud free area. For T1 α is small except for α_{nr} in the STERAO (Fig. 4d) and the ARM BUB case (Fig. 4c), i.e. if large scale forcings are

applied together with small random perturbations, retained as well as released highly soluble tracers are not efficiently transported from the boundary layer, neither for the tropical oceanic case nor for the mid-latitude continental case, which is characterized by more vigorous deep convection. The relative difference between α_r and α_{nr} in Table 1 is, however, large, indicating that the retention coefficient may be important for highly soluble trace gases for which even inefficient transport could play a role. Relatively large average upper tropospheric mixing ratios of highly soluble non-retained tracers with initial profile T1 were only found for cases in which deep convection was initialized by bubbles (which is consistent with results from earlier studies using cloud resolving models). The reason for this apparent dependence of the results on the model setup is discussed in the next section.

5 Influences of cloud dynamics and microphysics

Figure 6 shows time and horizontally domain averaged simulated hydrometeor mixing ratios for all sensitivity runs and the mixing ratios (per mass of dry air) of the non-retained tracer T1 taken up by hydrometeors. When bubbles were used to initiate deep convection, the amount of cloud water (Figs. 6c and d) and of trace gas dissolved in cloud droplets (Figs. 6g and h) is very low below about 2 km. For the ARM A LSF run on the other hand, higher cloud droplet mixing ratios tended to form in the inflow regions of the storms ("arcus clouds", marked by an "X" in Figs. 7b and c), which are absent in the STERAO case (Figs. 8b and d). In the LSF runs T1 did not reach the upper troposphere once it was taken up in cloud water at low levels (Figs. 6e and f). This indicates that the different dynamics in the inflow regions are responsible for the more efficient scavenging of the non-retained tracer in the LSF runs. This result differs from our initial hypothesis that freezing of cloud droplets at high altitudes inside the rapidly rising bubble prior to the onset of precipitation could be responsible for the higher sensitivities to the retention coefficient in the bubble runs. We did, however, not find any indication that surface precipitation sets in significantly earlier in the LSF runs

when compared to the bubble runs. Time series of the grid point maximum vertical velocity (indicating the presence of strong updrafts) and of the surface precipitation for the ARM A LSF run and the STERAO run are shown in Fig. 9. Despite the low temporal resolution of 30 min, the time series indicates that surface precipitation tends to lag the formation of updrafts in the ARM A LSF as well as in the STERAO run. Note also that efficient uptake of highly soluble trace gases in the cloud inflow has previously been found in the early cloud resolving model study by Wang and Chang (1993).

The hydrometeor mixing ratio profiles from the ARM BUB model run in Fig. 6 indicate that the cloud top did not reach above 12 km. Without applying a large scale forcing in this simulation, the relativly warm bubble resulted in realtively short lived single cell storm, as previously noted. Note also, that in the STERAO model run (Fig. 8), the anvil consists mostly of graupel (ρ_g=400 kg m^{-3}). The microphysics scheme used by Barth et al. (2001), on the other hand, did not include graupel, but hail (ρ_h=900 kg m^{-3}) as a category. In their STERAO simulations, the anvil consists mostly of snow. Their results regarding the role of the retention coefficient are, however, similar to the results from the STERAO run in this study.

6 Additional sensitivity runs and discussion

Mari et al. (2000) have suggested that inefficient scavenging of hydrogen peroxide (H_2O_2) in glaciated clouds may explain the observations of enhanced H_2O_2 in outflow from tropical deep convection during TRACE-A and elsewhere (Lee et al., 1997; Jaeglé et al., 1997). T1 and T2, on the other hand, were not transported to the upper troposphere efficiently in the LSF runs, independent of whether complete release from freezing hydrometeors was assumed. However, neither T1 nor T2 is representative of typical tropical H_2O_2 profiles. H_2O_2 is photochemically produced mostly in the lower and mid-tropsphere, mainly from the reaction of two hydroperoxy radicals:

$$HO_2 + HO_2 \xrightarrow{O_2,M} H_2O_2 + O_2 \quad (13)$$

Even in the upper troposphere, where the convective transport of methyl-hydroperoxide (CH_3OOH) is an important HO_x source, the chemical production of H_2O_2 can outweigh its photochemical loss, resulting in a small net photochemical production (Jaeglé et al., 2000; Salzmann, 2005). Observed tropical H_2O_2 profiles often show relatively high mixing ratios up to 5 or even 8 km altitude, and much lower values at the tropopause (see e.g. Heikes et al., 1996). In order to investigate the transport of tracers with more "H_2O_2–like" initial profiles, a set of 2-D model runs was performed for TOGA COARE. (The cost of multi-day 3-D simulations is unfortunately still relatively high, and T1 and T2 were mainly chosen to facilitate comparisons with previous studies of idealized soluble tracer transport.) The grid length in the 2-D runs is 500 km and the domain is oriented in East-West direction. The horizontal resolution and the vertical grid are identical to those in the 3-D simulations. Results from 2-D simulations of the meteorology during TOGA COARE can for example be found in Salzmann et al. (2004). The results for T1 and T2 in Fig.10a are qualitatively similar to the corresponding results from the 3-D runs (Fig. 4a), allowing us to have some confidence in the results of the 2-D runs, at least on a qualitative bases. (Note that a detailed comparison of 3-D and 2-D runs is considered outside the scope of this paper.)

Results for four additional initial profiles are shown in Fig. 10b and c. T3 and T5 are similar to T1 with constant mixing ratios up to 5 and 8 km, respectively, and zero mixing ratios above. T4 and T6 are identical to T2 below 5 and 8 km, respectively, while above, the "background" mixing ratio was reduced significantly to 10 nmol mol^{-1}. Release of "T3 released" from freezing hydrometeors in the upper troposphere is relatively inefficient. The simulated domain averaged upper tropospheric mixing ratio of "T4 released" is close to its initial value. This is a consequence of the competition between upward transport of "depleted air" (air in which the tracer mixing ratio has been depleted by scavenging) on the one hand, and release and upward transport on the other hand. For "T6 released", release and upward transport dominate, leading to significant increases of upper tropospheric mixing ratios. For "T6 retained", on the other hand, the upward transport of "depleted air" dominates. This is illustrated in Fig. 11c

and b for a large convective system with a relatively new convective tower in the East, and decaying deep convection to the West. While the insoluble tracer in Fig. 11a is transported to the upper troposphere resulting in outflow beyond the q_{totm} contour, "T6 retained" in Fig. 11b is scavenged, and low tracer mixing ratios are found in the outflow. (Note again that uptake by ice from the gas phase is not considered.) A considerable fraction of "T6 released" (Fig. 11c), on the other hand, is transported to the upper troposphere. However, not all storms show the same transport of "T6 released". In the western storm (at x=50–180 km) in Fig. 12, "T6 released" was scavenged, while in another storm previously located to the East of this storm (also shown in Fig. 12), it was partially transported. This implies that some "competition" between different storms takes place, which plays a role for the domain averaged upper tropospheric mixing ratios.

While "T6 released" is transported to the upper troposphere in deep convection, scavenging prevents efficient transport of highly soluble tracers from below about 5 km (T3 and T4 in Fig 10b), where rain mixing ratios are high (Fig. 6a). This indicates that for TOGA COARE inefficient scavenging of H_2O_2 in the glaciated part of the storms in combination with a source between 5 and 8 km can indeed contribute to increased observed upper tropospheric mixing ratios, supporting the hypothesis of Mari et al. (2000).

Unfortunately, very large uncertainty still exists about the retention coefficient of H_2O_2, despite recent efforts to explain the large range of values (from almost zero to one) from a number of laboratory studies (Stuart and Jacobson, 2004). Efforts to better determine retention coefficients of important trace gases for various processes and under different conditions are underway, for example within the framework of the TROPEIS (The Tropospheric Ice Phase) project, which is funded by the German Research Foundation (DFG). Furthermore, it is still largely uncertain to what extent H_2O_2 is taken up on ice directly from the gas phase.

An important uncertainty (e.g. Wurzler, 1997) in the model is due to the usage of a single moment (or "bulk") microphysics scheme in which the size-distributions of rain

drops, graupel, and snow are diagnosed assuming exponential (Marshall-Palmer) size distributions. Unfortunately, using size resolving microphysics schemes increases the computational cost drastically, so that such schemes have mainly been used in models with very simplified storm dynamics. Furthermore, the observational data needed for evaluating the details of various microphysics schemes under different conditions is still limited, leading to an additional uncertainty in calculations of soluble tracer transport and scavenging.

A very important question remaining is whether the results of the LSF runs are representative of most storms. Under summertime conditions, warm air bubbles are known to form over land due to differential surface heating. The rising of these bubbles can then initiate thunderstorms. Furthermore, it can not completely be ruled out that artifacts occur in the LSF runs, e.g. due to the homogeneous nudging of the u and v wind components, although there is no obvious reason why this should happen. Differences in cloud base height between different thunderstorms may also play a role. In Colorado, where the STERAO campaign was conducted, thunderstorms can have fairly high cloud bases above ground. On the other hand, initiating numerical models by bubbles of arbitrary size and strength has disadvantages as well. In Fig. 8d, the signature of the three thermals which were used to initiate deep convection in the STERAO case can still be seen very clearly. In the future more sophisticated setups like the one used by Stenchikov et al. (2005) and DeCaria et al. (2005), who applied horizontally non-uniform initial conditions for their simulation of a 12 July STERAO storm and took into account terrain interactions, could help to overcome these problems. Another promising option is the use of high resolution nested models or models with non-uniform horizontal grid spacings with relatively realistic land surface models. While the land surface model allows the formation of warm bubbles, nesting in principle allows the model to take into account the the influences of larger scale circulations, which are currently not resolved in limited domain cloud resolving models. Some first attempts by the authors at simulating the TOGA COARE case using multiply nested grids in the WRF model and a nudging technique for the coarsest grid provide a rea-

son to be optimistic that nested models can be used in regions in which the large scale dynamics play an important role (in TOGA COARE especially the Hadley and Walker circulation, and the Intra-Seasonal Oscillation (e.g. Madden and Julian, 1994)).

This study has been limited to idealized tracers. The advantage of this approach is that they allow to understand sensitivities which are difficult to investigate based on simulations of realistic trace gases. The disadvantage of idealized tracers is, however, that they are by definition not necessarily representative of realistic tracers. Furthermore, as an initial step, this study explicitly focuses on highly soluble tracers which were found to have considerably more complicated behavior than we anticipated based on previous studies. As a future step, extending this study to moderately soluble tracers may definitely be interesting.

Last but not least, it should be noted that currently no theoretical framework is readily available for treating reversible exchange of trace gases between the surfaces of frozen hydrometeors and the gas phase at the same time as the possible retention of trace gases due to "burial" in ice hydrometeors in cloud resolving model simulations. If efficient direct uptake on ice from the gas phase were considered in this study, one would expect the large sensitivity towards the retention coefficient found in the "bubble" runs to decrease.

7 Summary and conclusions

It was shown that different cloud droplet mixing ratios in association with different dynamics in the inflow regions can have large effects on the sensitivity of the vertical transport of highly soluble trace gases towards the retention coefficient. High cloud water mixing ratios in the inflow regions were found in the cases in which LSF was applied, but not in the cases in which deep convection was initiated by bubbles. It is therefore concluded that the vertical transport of non retained highly soluble trace gases may be significantly less efficient than suggested by previous model studies in which bubbles were used to initiate deep convection. In the LSF runs scavenging is

found to almost entirely prevent a highly soluble tracer initially located in the lowest 1.5 km of the troposphere from reaching the upper troposphere, independent of the retention coefficient for both the TOGA COARE and the ARM case.

A tracer with a high initial mixing ratio up to an altitude of 8 km, and a low "background" above 8 km (T6), on the other hand, was efficiently transported to the upper troposphere if it was assumed to be completely released from hydrometeors upon freezing. This indicates that inefficient scavenging of H_2O_2 in the glaciated part of tropical storms in combination with an upper air chemical source can contribute to observed increases in its upper tropospheric mixing ratios in deep convective outflow. If complete retention was assumed for T6, the upward transport of tracer-poor air (from which the tracer has been largely scavenged) in association with downwards transport of tracer-rich air lead to a decrease of the domain averaged mixing ratios of T6 in the upper troposphere.

For a comparable tracer with a higher "background" mixing ratio above 8 km (T2), the upper tropospheric mixing ratios were decreased by deep convection, independent of the retention coefficient. The magnitude of the decrease was, however, strongly dependent on the retention coefficient. This suggests, that the retention coefficient plays a large role for the scavenging of highly soluble trace gases with a (chemical) source in the middle and upper troposphere. Whether release and transport on average leads to an increase of upper tropospheric mixing ratios by deep convection or whether scavenging is more important for a non-retained highly soluble tracer depends on the altitude of the (photochemical) source and on the ratio of lower and mid-tropospheric to upper tropospheric mixing ratios. Large differences were not only found for different initial profiles, but also between individual storms.

Given the apparent dependence of the results on the model setup (LSF vs. "bubble"), one could argue that in the future more studies with different approaches (especially with a more realistic initiation of deep convection, e.g. considering effects of orography) are needed. Such studies as well as the use of size resolved microphysics schemes without the constraint of strongly idealized storm dynamics will be facilitated by increas-

ACPD
6, 10773–10809, 2006

ing computer power. For assessing potential influences of the release of H_2O_2 from freezing hydrometeors on the upper tropospheric HO_x budget, additional laboratory studies are necessary in order to better determine the retention coefficient of H_2O_2 for freezing and riming processes under various conditions as well as additional in-situ observations in deep convective outflow in association with detailed model studies.

Acknowledgements. We appreciate valuable discussions on this topic with many colleagues, especially with R. von Kuhlmann, B. Bonn, and with several colleagues from the TROPEIS Collaborative Research Centre. The work was supported by funding from the German Research Foundation (DFG) Collaborative Research Centre 641 (SFB 641) "The Tropospheric Ice Phase (TROPEIS)".

References

Barth, M. C., Stuart, A. L., and Skamarock, W. C.: Numerical simulations of the July 10, 1996, Stratospheric-Tropospheric Experiment: Radiation, Aerosols, and Ozone (STERAO)-Deep Convection Experiment storm: Redistribution of soluble tracers, J. Geophys. Res., 106, 12 381–12 400, 2001. 10775, 10779, 10781, 10783, 10784, 10786

Chatfield, R. B. and Crutzen, P. J.: Sulfur dioxide in remote oceanic air: Cloud transport of reactive precursors, J. Geophys. Res., 89, 7111–7132, 1984. 10774, 10775

Chou, M.-D., Suarez, M. J., Ho, C.-H., Yan, M. M.-H., and Lee, K.-T.: Parameterizations for cloud overlapping and shortwave single-scattering properties for use in general circulation and cloud ensemble models, J. Climate, 11, 202–214, 1998. 10776

Crutzen, P. J. and Lawrence, M. G.: The impact of precipitation scavenging on the transport of trace gases: A 3-dimensional model sensitivity study, J. Atmos. Chem., 37, 81–112, 2000. 10775, 10784

DeCaria, A. J., Pickering, K. E., Stenchikov, G. L., and Ott, L. E.: Lightning generated NO_x and its impact on tropospheric ozone production: A 3-D modeling study of a STERAO-A thunderstorm, J. Geophys. Res., 110, D14303, doi:10.1029/2004JD005556, 2005. 10789

Dickerson, R. R., Huffman, G. J., Luke, W. T., Nunnermacker, L. J., Pickering, K. E., Leslie, A. C. D., Lindsey, C. G., Slinn, W. G. N., Kelly, T. J., Daum, P. H., Delaney, A. C., Greenberg,

J. P., Zimmerman, P. R., Boatman, J. F., Ray, J. D., and Stedman, D. H.: Thunderstorms: An important mechanism in the transport of air pollutants, Science, 235, 460–465, 1987. 10774

Diehl, K., Mitra, S. K., and Pruppacher, H. R.: A laboratory study of the uptake of HNO_3 and HCl vapor by snow crystals and ice spheres at temperatures between 0 and –40°C, Atmos. Environ., 29, 975–981, 1995. 10780

Gregory, D. and Guichard, F.: Aspects of the parameterization of organized convection: Contrasting cloud resolving model and single-column model realizations, Q. J. R. Meteorol. Soc., 128, 625–646, 2002. 10781

Hales, J. M. and Dana, M. T.: Precipitation scavenging of urban pollutants by convective storm systems, J. Appl. Meteorol., 18, 294–316, 1979. 10775

Heikes, B., Lee, M., Jacob, D., Talbot, R., Bradshaw, J., Singh, H., Blake, D., Anderson, B., Fuelberg, H., and Thompson, A. M.: Ozone, hydroperoxides, oxides of nitrogen, and hydrocarbon budgets in teh marine boundary layer over the South Atlantic, J. Geophys. Res., 101, 24 221–24 221, 1996. 10787

Isaac, G. A. and Joe, P. I.: The vertical transport and redistribution of pollutants by clouds, in: The Meteorology of Acid Deposition, edited by: Samson, P. J., Air Pollution Control Association, Pittsburg, PA, USA, 496–512, 1983. 10774

Jaeglé, L., Jacob, D. J., Wennberg, P. O., Spivakovsky, C. M., Hanisco, T. F., Lanzendorf, E. J., Hinsta, E. J., Fahey, D. W., Keim, E. R., Proffit, E. R., Atlas, M. H., Flocke, E. L., Schauffer, S., McElroy, C. T., Midwinter, C., Pfister, L., and Wilson, J. C.: Observed OH and HO_2 in the upper troposphere suggest a major source from convective injection of peroxides, Geophys. Res. Lett., 24, 3181–3184, 1997. 10775, 10786

Jaeglé, L., Jacob, D. J., Brune, W. H., Faloona, I., Tan, D., Heikes, B. G., Kondo, Y., Sachse, G. W., Anderson, B., Greogory, G. L., Singh, H. B., Pueschel, R., Ferry, G., Blake, D. R., and Shetter, R. E.: Photochemistry of HO_x in the upper troposphere at northern midlatitudes, J. Geophys. Res., 105, 3877–3892, 2000. 10787

Johnson, D. E., Tao, W.-K., Simpson, J., and Sui, C.-H.: A study of the response of deep tropical clouds to large-scale thermodynamic forcings. Part I: Modeling strategies and simulations of TOGA COARE convective systems, J. Atmos. Sci., 59, 3492–3518, 2002. 10781

Krueger, S. K., Fu, Q., Liou, K. N., and Chin, H.-N. S.: Improvements of an ice-phase microphysics parameterization for use in numerical simulations of tropical convection, J. Appl. Meteorol., 34, 281–287, 1995. 10776

Lee, M., Heikes, B. G., Sachse, G., and Anderson, B.: Hydrogen peroxide, organic hydroperox-

ide, and formaldehyde as primary pollutants from biomass burning, J. Geophys. Res., 102, 1301–1309, 1997. 10786
Lin, Y.-L., Farley, R. D., and Orville, H. D.: Bulk parameterization of the snow field in a cloud model, J. Climate Appl. Meteorol., 2, 1065–1092, 1983. 10776
Lord, S. J., Willoughby, H. E., and Piotrowicz, J. M.: Role of a parameterized ice-phase microphysics in an axisymmetric, nonhydrostatic tropical cyclone model, J. Atmos. Sci., 42, 2836–2848, 1984. 10776
Madden, R. A. and Julian, P. R.: Observations of the 40–50 day tropical oscillation – A review, Mon. Weather Rev., 122, 814–836, 1994. 10790
Mari, C., Jacob, D. J., and Bechtold, P.: Transport and scavenging of soluble gases in a deep convective cloud, J. Geophys. Res., 105, 22 255–22 267, 2000. 10775, 10786, 10788
Massman, W. J.: A review of the molecular diffusivities of H_2O, CO_2, CH_4, SO_2, NH_3, N_2O, NO, and NO_2 in air, O_2 and N_2 near STP, Atmos. Environ., 32, 1111–1127, 1998. 10778, 10779
Mlawer, E. J., Taubman, S. J., Brown, P. D., Iacono, M. J., and Clough, S. A.: Radiative transfer for inhomogeneous atmosphere: RRTM a validated correlated-k model for the longwave, J. Geophys. Res., 102, 16 663–16 682, 1997. 10776
Prather, M. J. and Jacob, D. J.: A persistent imbalance in HO_x and NO_x photochemistry of the upper troposphere driven by deep tropical convection, Geophys. Res. Lett., 24, 3189–3192, 1997. 10775
Pruppacher, H. R. and Klett, J. D.: Microphysics of clouds and precipitation, Kluwer, Dordrecht, 1997. 10779
Salzmann, M.: Influences of deep convective cloud systems on tropospheric trace gases and photochemistry over the tropical West Pacific: A modeling case study, Ph.D. thesis, Johannes Gutenberg-Universität Mainz, Mainz, Germany, http://nbn-resolving.de/urn/resolver.pl?urn=urn:nbn:de:hebis:77-9470, 2005. 10787
Salzmann, M., Lawrence, M. G., Phillips, V. T. J., and Donner, L. J.: Modelling tracer transport by a cumulus ensemble: Lateral boundary conditions and large-scale ascent, Atmos. Chem. Phys., 4, 1797–1811, 2004. 10781, 10782, 10787
Schwartz, S. E.: Mass-transport considerations pertinent to aqueous phase reactions of gases in liquid-water clouds, Pages 415–471 of: Chemistry of Multiphase Atmospheric Systems, edited by: Jaeschke, W., Springer-Verlag, Berlin and Heidelberg, Germany, 1986. 10778
Skamaraock, W. C., Klemp, J. B., and Dudhia, J.: Prototypes for the WRF (Weather Research and Forecasting) model, in: Preprints, Ninth Conf. Mesoscale Processes, pp. J11–J15, Amer.

Meteorol. Soc., Fort Lauderdale, FL, 2001. 10776
Skamarock, W. C., Powers, J. G., Barth, M., Dye, J. E., Matejka, T., Bartels, D., Baumann, K., Stith, J., Parrish, D. D., and Hubler, G.: Numerical simulations of the July 10 Stratospheric-Tropospheric Experiment: Radiation, Aerosols, and Ozone/Deep Convection Experiment convective system: Kinematics and transport, J. Geophys. Res., 105, 19 973–19 990, 2000. 10783
Soong, S.-T. and Ogura, Y.: Response of tradewind cumuli to large-scale processes, J. Atmos. Sci., 37, 2035–2050, 1980. 10780
Stenchikov, G. L., Pickering, K. E., DeCaria, A. J., Tao, W.-K., Scala, J., Ott, L., Bartels, D., and Matejka, T.: Simulation of the fine structure of the 12 July 1996 Stratosphere-Troposphere Experiment: Radiation, Aerosols and Ozone (STERAO-A) storm accounting for the effects of terrain and interaction with mesoscale flow, J. Geophys. Res., 110, D14304, doi:10.1029/2004JD005582, 2005. 10789
Stuart, A. L. and Jacobson, M. Z.: Chemical retention during dry growth riming, J. Geophys. Res., 109, D07305, doi:10.1029/2003JD004197, 2004. 10788
Takemi, T. and Rotunno, R.: The effects of subgrid model mixing and numerical filtering in simulations of mesoscale cloud systems, Mon. Weather Rev., 131, 2085–2191, 2003. 10777
Walcek, C. J.: Minor flux adjustment near mixing ratio extremes for simplified yet highly accurate monotonic calculation of tracer advection, J. Geophys. Res., 105, 9335–9348, 2000. 10776
Wang, C. and Chang, J. S.: A three-dimensional numerical model of cloud dynamics, microphysics, and chemistry: 3. Redistribution of pollutants, J. Geophys. Res., 98, 16 787–16 798, 1993. 10786
Wang, C. and Crutzen, P. J.: Impact of a simulated severe local storm on the redistribution of sulfur dioxide, J. Geophys. Res., 100, 11 357–11 367, 1995. 10775
Webster, P. J. and Lukas, R.: TOGA COARE: The Coupled Ocean-Atmosphere Response Experiment, Bull. Am. Meteorol. Soc., 73, 1377–1416, 1992. 10781
Wicker, L. J. and Skamarock, W. C.: Time-splitting methods for elastic models using forward time schemes, Mon. Weather Rev., 130, 2088–2097, 2002. 10776
Wurzler, S.: The scavenging of nitrogen compounds by clouds and precipitation: Part II. The effects of cloud microphysical parameterization on model predictions of nitric acid scavenging by clouds, Atmos. Ocean, 47–48, 219–233, 1997. 10788
Xu, K.-M. and Randall, D.: Explicit simulation of cumulus ensembles with GATE phase III data: Comparison with observations, J. Atmos. Sci., 53, 3710–3736, 1996. 10780

Xu, K.-M., Cederwall, R. T., Donner, L. J., Grabowski, W. W., Guichard, F., Johnson, D. E., Khairoudtdinov, M., Krueger, S. K., Petch, J. C., Randall, D. R., Seman, C. J., Tao, W.-K., Wang, D., Xie, S. C., Yio, J. J., and Zhang, M.-H.: An intercomparison of cloud-resolving models with the Atmospheric Radiation Measurement summer 1997 Intensive Observation Period data, Q. J. R. Meteorol. Soc., 128, 593–624, 2002. 10782

Yin, Y., Carslaw, K. S., and Parker, D. J.: Redistribution of trace gases by convective clouds - mixed phase processes, Atmos. Chem. Phys., 2, 293–306, 2002. 10775

Zhang, M.-H., Lin, J. L., Cederwall, R. T., Yio, J. J., and Xie, S. C.: Objective analysis of ARM IOP data: Method, feature, and sensitivity, Mon. Weather Rev., 129, 295–311, 2001. 10782

Table 1. Ratios $\alpha=\overline{\mu}_s/\overline{\mu}_i$, where $\overline{\mu}_s$ and $\overline{\mu}_i$ are the horizontally domain averaged mixing ratios in the upper troposphere of highly soluble and insoluble tracers, respectively, for two different initial profiles (T1 and T2) for TOGA COARE (T.C.), ARM A, and STERAO.

	T.C. 2.5 h[2]	T.C. 12 h[3]	T.C. 24 h[3]	ARM 2.5 h[2]	ARM 12 h[3]	ARM 24 h[3]	STERAO	ARM BUB
α_r[1] T1	7.0×10^{-4}	2.1×10^{-4}	1.2×10^{-4}	1.1×10^{-3}	1.2×10^{-3}	1.0×10^{-3}	1.8×10^{-2}	3.4×10^{-2}
α_{nr} T1	2.4×10^{-2}	1.0×10^{-2}	9.7×10^{-3}	7.2×10^{-2}	6.6×10^{-2}	8.4×10^{-2}	0.90	0.55
α_r T2	0.84	0.52	0.32	0.998	0.67	0.48	0.88	0.996
α_{nr} T2	0.91	0.67	0.48	0.998	0.76	0.61	0.98	0.999

[1] Soluble tracers are either assumed to be completely retained (α_r) or completely released (α_{nr}).
[2] 2.5 h after the onset of deep convection (defined as the first output time when the total hydrometeor mixing ratio $q_{\text{totm,max}} = q_{\text{cloudwater}} + q_{\text{cloudice}} + q_{\text{rain}} + q_{\text{graupel}} + q_{\text{snow}}$ at a single grid point above 7 km exceeds 1 g kg^{-1}) for each 24 h time slice.
[3] After the beginning of each 24 h time slice.

ACPD
6, 10773–10809, 2006

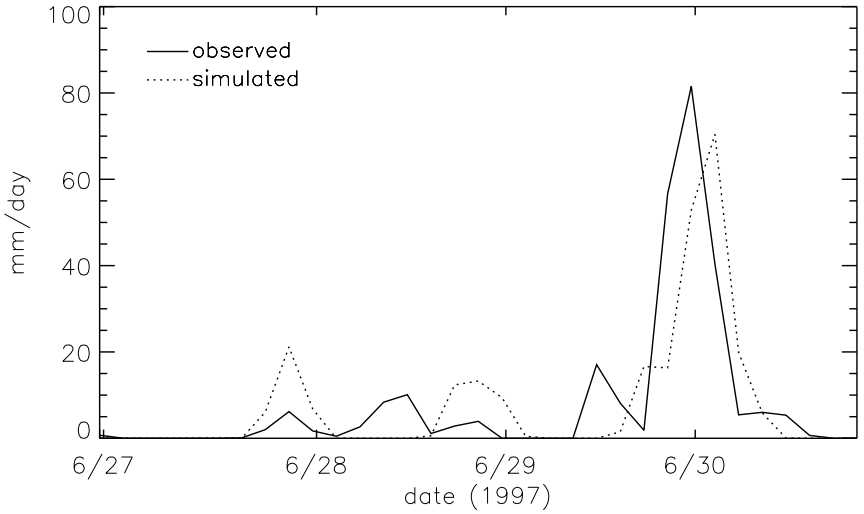

Fig. 1. Time series of modeled and observed 6 h average surface precipitation rates for the ARM A LSF simulation.

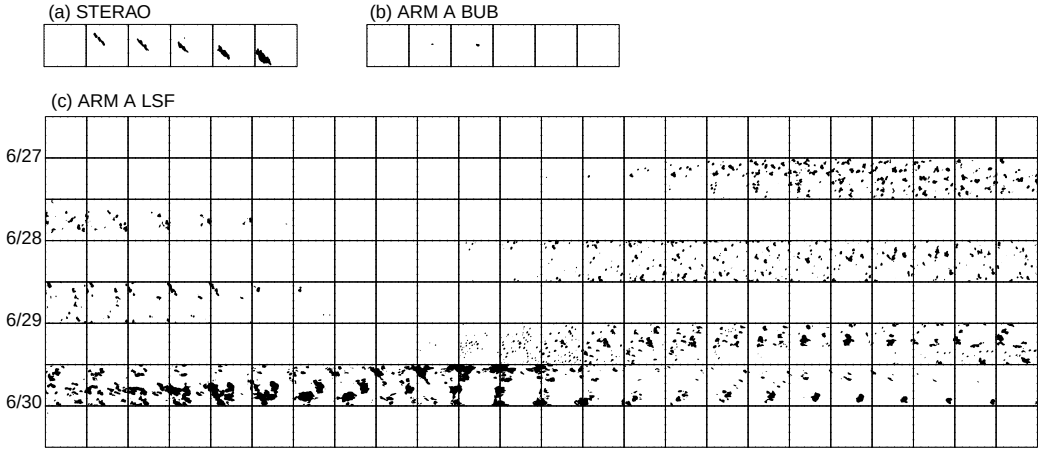

Fig. 2. Series of x-y contour plots: 1 mm h^{-1} filled contour of simulated rainfall rates. The interval between the individual plots is 30 min; in **c** each row represents one half day. The x-axis are directed in W-E direction, and the y-axis in S-N direction.

ACPD
6, 10773–10809, 2006

EGU

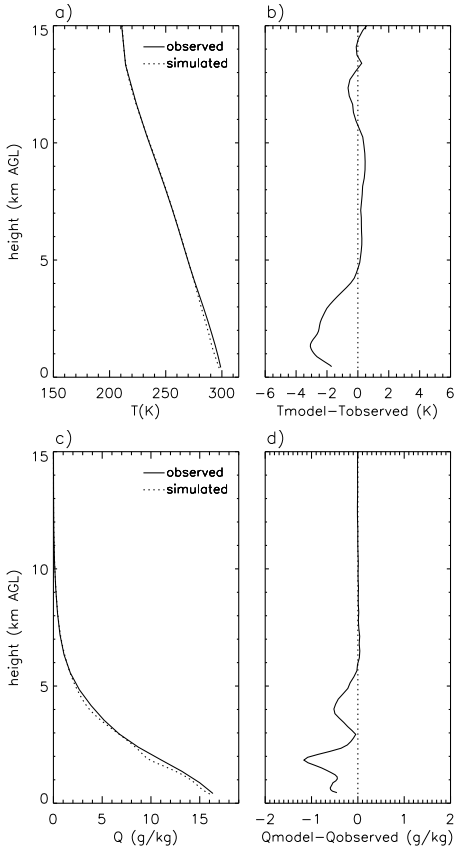

Fig. 3. Vertical profiles of modeled and observed domain and time averaged temperatures and water vapor mixing ratios.

ACPD
6, 10773–10809, 2006

EGU

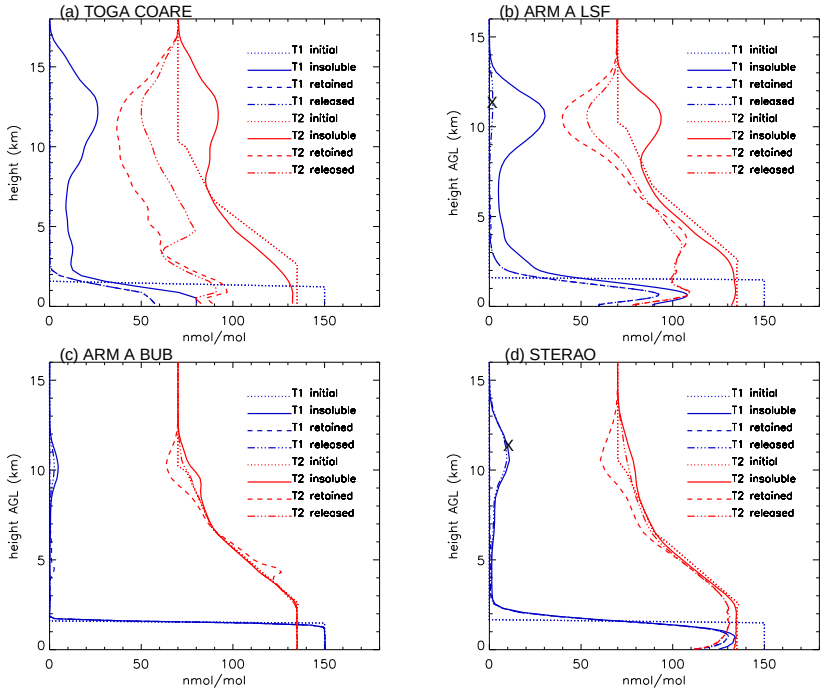

Fig. 4. Initial tracer profiles and horizontally domain averaged mixing ratios 12 h after the beginning of each 24 h time slice **(a)** for the TOGA COARE run (6 time slices) and **(b)** for the ARM A LSF run (3 time slices). **(c)** Initial tracer profiles and horizontally averaged mixing ratios at the end of the ARM A BUB run. For better readability (i.e. increased spacing between the individual lines) the mixing ratios in (c) were averaged over a $28 \times 30\,\mathrm{km}^2$ sub-domain at the western edge of the domain centered at the gridpoint (i, j)=124, 55, where the main outflow at is located after 2.5 h **(d)**. Initial tracer profiles and horizontally domain averaged mixing ratios at the end of the STERAO simulation after 2.5 h . Note the large difference between (b) and (d) of "T1 released" in the upper troposphere in the region marked by an "X".

ACPD
6, 10773–10809, 2006

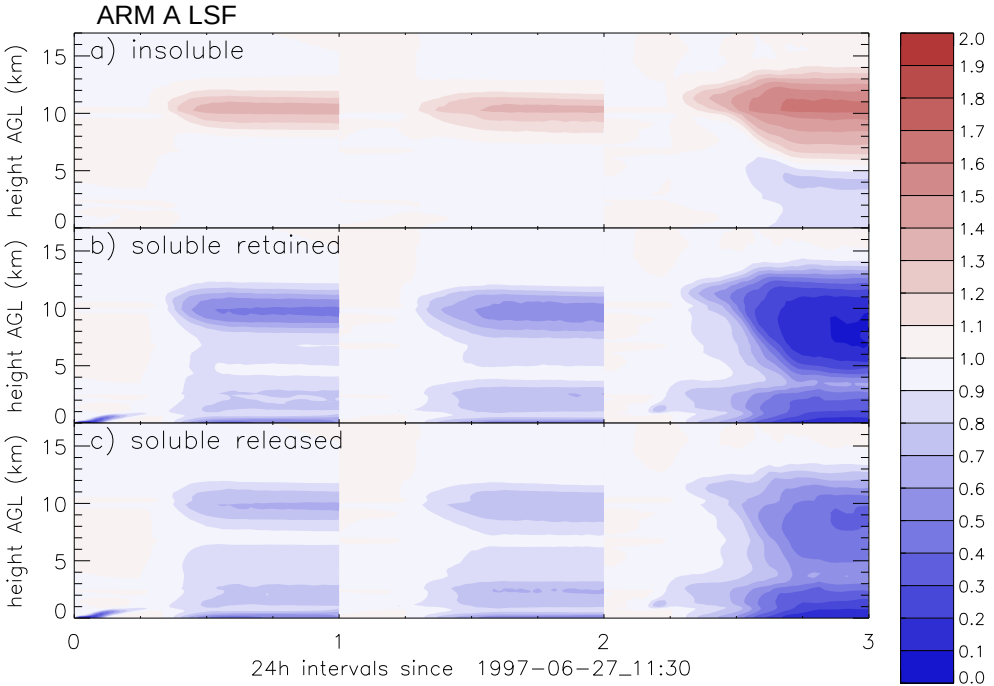

Fig. 5. Time series of the ratio β of modeled averaged mixing ratio to initial mixing ratio for tracers with initial profile T2 during the ARM A episode (excluding the first and the last 12 h of the simulation). Note that β never exceeds one if the tracer is assumed to be highly soluble.

ACPD
6, 10773–10809, 2006

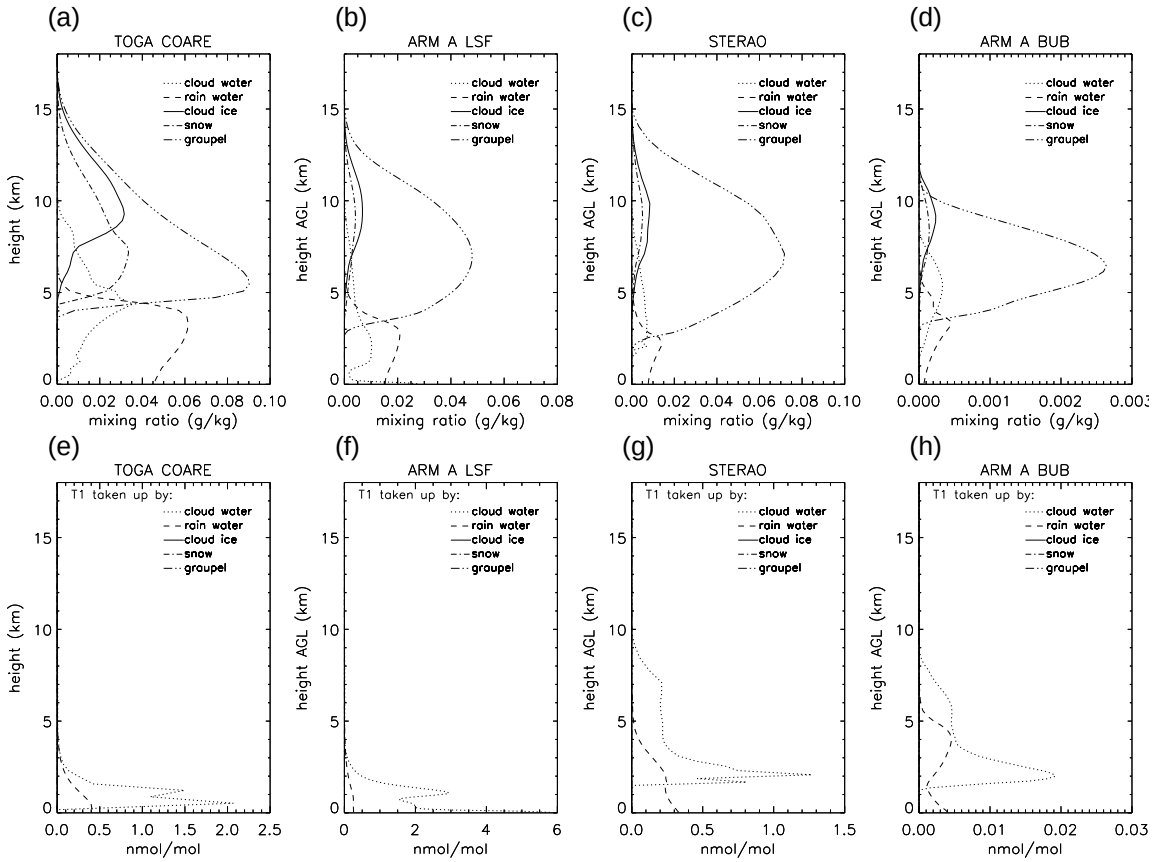

Fig. 6. Simulated time and horizontally domain averaged **(a)**–**(d)** hydrometeor mixing ratios and **(e)**–**(h)** mixing ratios (per mass of dry air) of non-retained tracer T1 taken up by hydrometeors.

ACPD
6, 10773–10809, 2006

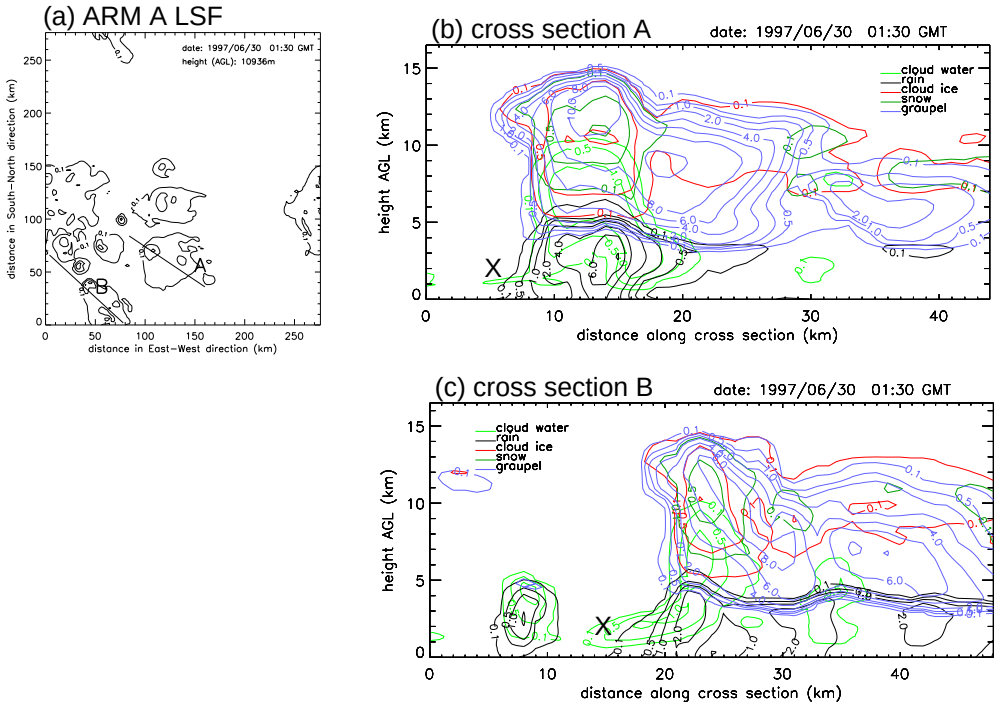

Fig. 7. (a) Cloud ice mixing ratio contours for the ARM A LSF run at about 11 km above ground level on 30 June, 1:30 UTC and locations of cross sections in **(b)** and **(c)**; (b) and (c): cross sections of hydrometeor mixing ratios with contour levels 0.1, 0.5, 1.0, 2.0, 4.0, 6.0, 8.0, 10.0. Note the high cloud water mixing ratios in the inflow region marked by an "X".

ACPD
6, 10773–10809, 2006

EGU

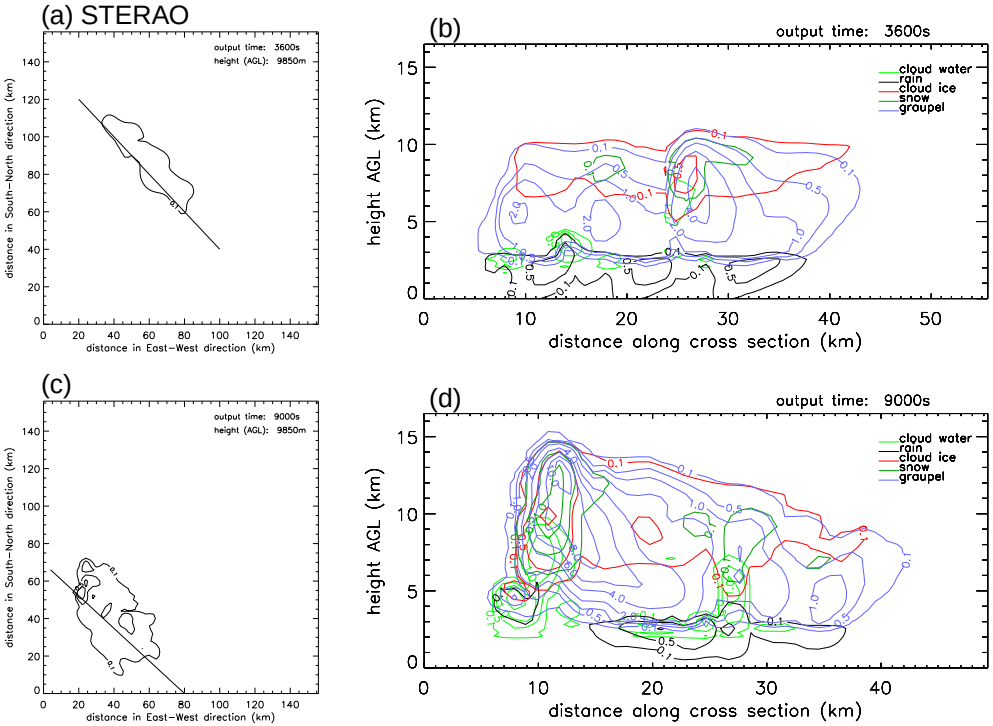

Fig. 8. **(a)** and **(c)** Cloud ice mixing ratio contours for the STERAO case at 9850 m above ground level after 3600 s and after 9000 s and locations of cross sections in **(b)** and **(d)**; (b) and (d): Contour levels as in Fig. 7b.

ACPD
6, 10773–10809, 2006

EGU

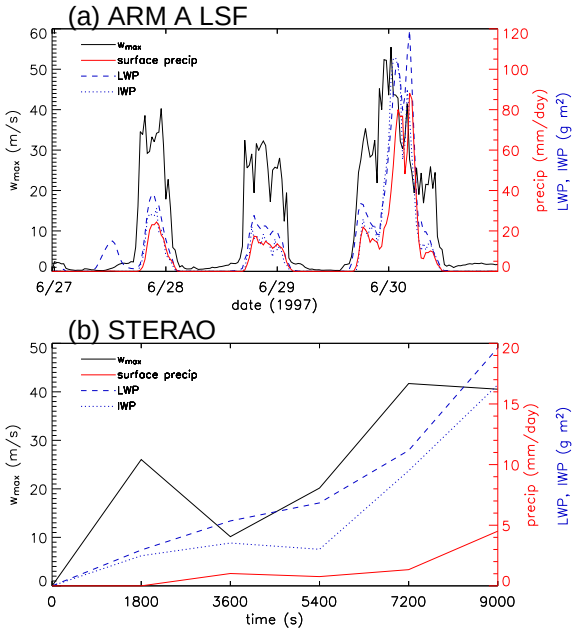

Fig. 9. Time series of domain maximum grid point vertical velocity, surface precipitation, and averaged liquid (LWP) and ice water path (IWP) sampled every 30 min for **(a)** ARM A LSF and **(b)** STERAO.

ACPD
6, 10773–10809, 2006

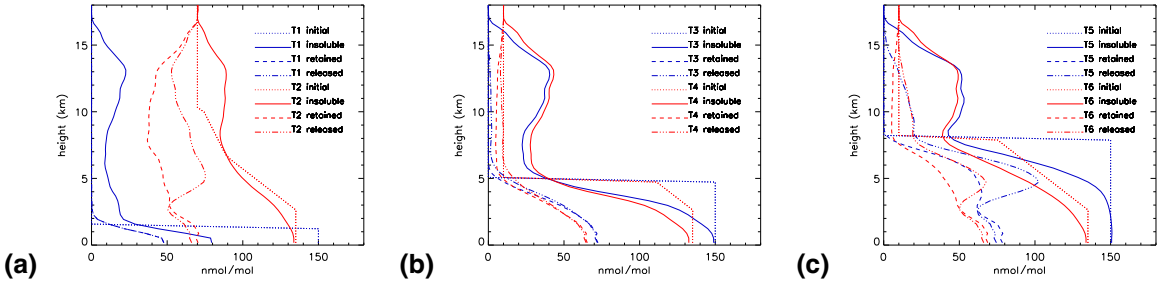

Fig. 10. (a) As Fig. 4a for the TOGA COARE 2-D run; **(b)** and **(c)** same as (a) for different initial tracer profiles.

ACPD
6, 10773–10809, 2006

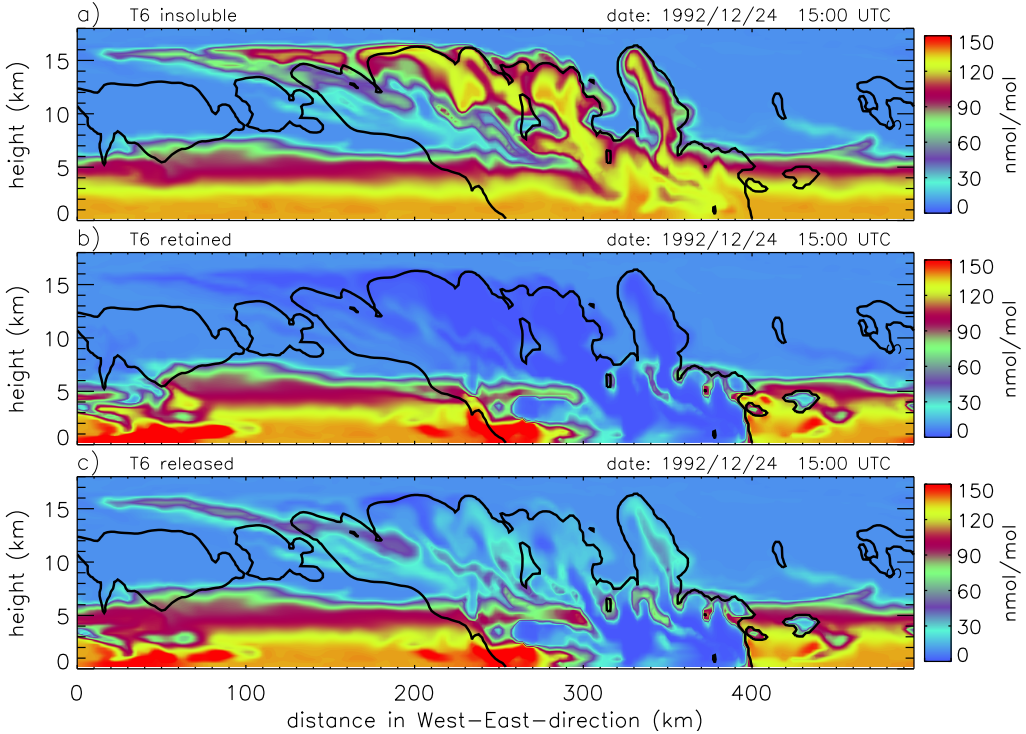

Fig. 11. Volume mixing ratio contours for tracers the with initial profile T6 **(a)** insoluble, **(b)** soluble retained, **(c)** soluble released, and q_{totm}<0.01 g kg^{-1} mass mixing ratio contour from the TOGA-COARE 2-D run for 24 December 1992, 15:00 UTC, where $q_{totm} = q_{cloudwater} + q_{cloudice} + q_{rain} + q_{graupel} + q_{snow}$.

ACPD
6, 10773–10809, 2006

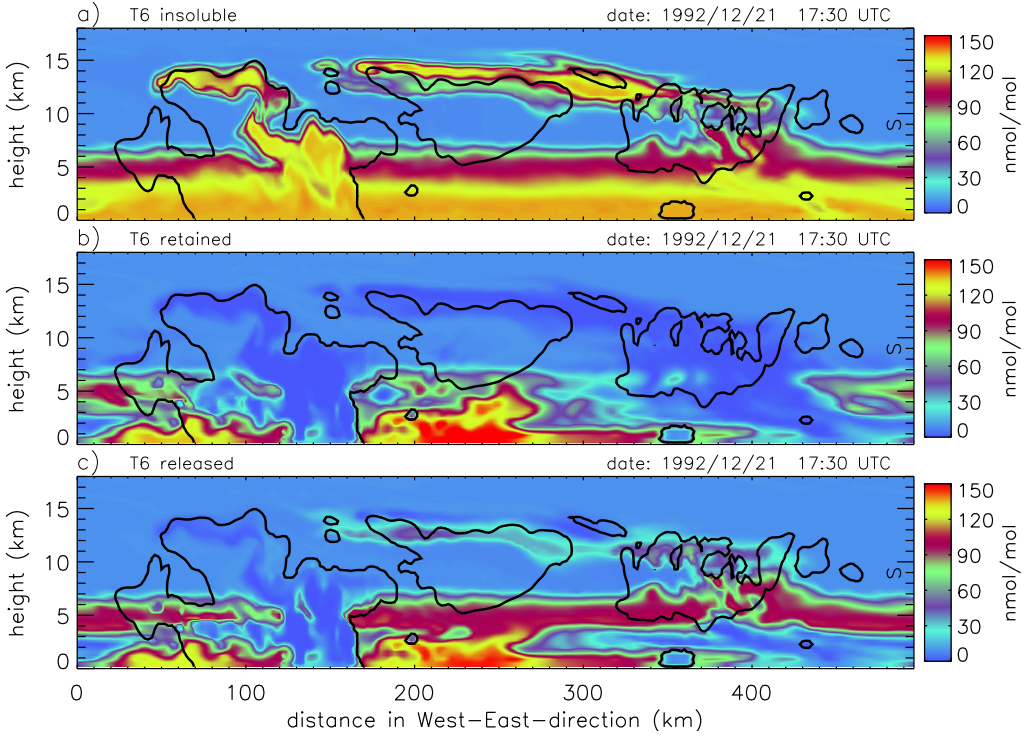

Fig. 12. Same as Fig. 11 for 21 December 1992, 17:30 UTC.

ACPD
6, 10773–10809, 2006

EGU